Vector form factor in K_{l3} semileptonic decay with two flavors of dynamical domain-wall quarks

Chris Dawson,[1] Taku Izubuchi,[1,2] Takashi Kaneko,[3,4] Shoichi Sasaki,[1,5] and Amarjit Soni[6]

[1]*RIKEN-BNL Research Center, Brookhaven National Laboratory, Upton, New York 11973, USA*
[2]*Institute for Theoretical Physics, Kanazawa University, Kanazawa, Ishikawa 920-1192, Japan*
[3]*High Energy Accelerator Research Organization (KEK), Tsukuba, Ibaraki 305-0801, Japan*
[4]*Graduate University for Advanced Studies, Tsukuba, Ibaraki 305-0801, Japan*
[5]*Department of Physics, University of Tokyo, Tokyo 113-0033, Japan*
[6]*Physics Department, Brookhaven National Laboratory, Upton, New York, 11973, USA*

(Received 4 August 2006; published 7 December 2006)

We calculate the vector form factor in $K \to \pi l \nu$ semileptonic decays at zero momentum transfer $f_+(0)$ from numerical simulations of two-flavor QCD on the lattice. Our simulations are carried out on $16^3 \times 32$ at a lattice spacing of $a \simeq 0.12$ fm using a combination of the DBW2 gauge and the domain-wall quark actions, which possesses excellent chiral symmetry even at finite lattice spacings. The size of fifth dimension is set to $L_s = 12$, which leads to a residual quark mass of a few MeV. Through a set of double ratios of correlation functions, the form factor calculated on the lattice is accurately interpolated to zero momentum transfer, and then is extrapolated to the physical quark mass. We obtain $f_+(0) = 0.968(9)(6)$, where the first error is statistical and the second is the systematic error due to the chiral extrapolation. Previous estimates based on a phenomenological model and chiral perturbation theory are consistent with our result. Combining with an average of the decay rate from recent experiments, our estimate of $f_+(0)$ leads to the Cabibbo-Kobayashi-Maskawa (CKM) matrix element $|V_{us}| = 0.2245(27)$, which is consistent with CKM unitarity. These estimates of $f_+(0)$ and $|V_{us}|$ are subject to systematic uncertainties due to the finite lattice spacing and quenching of strange quarks, though nice consistency in $f_+(0)$ with previous lattice calculations suggests that these errors are not large.

DOI: 10.1103/PhysRevD.74.114502 PACS numbers: 12.38.Gc

I. INTRODUCTION

There has recently been rapid progress in the precise determination of the elements of the Cabibbo-Kobayashi-Maskawa (CKM) matrix [1] leading towards a stringent test of its unitarity. Let us recall that such a test is a powerful method to search for new physics beyond the standard model. In particular $d \to u$ and $s \to u$ semileptonic transitions provide the most precise constraints on the size of the elements, and hence CKM unitarity on the first row

$$|V_{ud}|^2 + |V_{us}|^2 + |V_{ub}|^2 = 1 - \delta \tag{1}$$

can now be examined accurately [2,3].

The values quoted in the 2004 PDG [4]

$$|V_{ud}| = 0.9738(5), \qquad |V_{us}| = 0.2200(26), \qquad |V_{ub}| = (3.67 \pm 0.47) \times 10^{-3}, \tag{2}$$

lead to

$$\delta = 0.0033(15), \tag{3}$$

which deviates from zero by two σ. We have to improve the accuracy on δ in order to confirm whether this deviation is a genuine signal of unitarity violation. We note that $|V_{ub}|$ is so small that it can be safely neglected in this unitarity test. Since about half the error of δ comes from the uncertainty in $|V_{ud}|$, and another half from $|V_{us}|$, we need a more precise determination of both of these two elements. In the present paper, we focus on the determination of $|V_{us}|$.

We also note that $|V_{us}|$ gives the basic parameter λ in the Wolfenstein parameterization of the CKM matrix [5]. A precise determination of $|V_{us}|$ is, therefore, important also for phenomenological studies of CP violation processes based on this parametrization.

So far, $|V_{us}|$ has been determined from several processes: K_{l3} decays [4] which provide the value in Eq. (2), hyperon β decays [6], $K_{\mu 2}$ and $\pi_{\mu 2}$ decays [7], and hadronic τ decays [8]. At the moment, the K_{l3} decays provide the most precise determination among these, and its result has been quoted in the PDG. We, therefore, try to determine $|V_{us}|$ through the K_{l3} decays.

As will be explained in Sec. II, $|V_{us}|$ can be determined through experimental determination of the decay rate Γ and theoretical calculation of the vector form factor at zero momentum transfer $f_+(0)$. The two σ deviation from unitarity in Eq. (3) motivated recent measurements of Γ [9–13]. These experiments prefer a larger value for $|V_{us}|$, which is consistent with unitarity. However, a precise calculation of $f_+(0)$, say with an accuracy of 1%, is also indispensable in order to establish this consistency with unitarity.

A good theoretical control on $f_+(0)$ is provided by $SU(3)$ symmetry and the Ademollo-Gatto theorem [14]. The vector current conservation guarantees $f_+(0) = 1$ at zero momentum transfer [15], and then the Ademollo-Gatto theorem states that the $SU(3)$ breaking effects

$f_+(0) - 1$ start at second order in $(m_s - m_{ud})$, where m_{ud} represents the averaged mass of up and down quarks. This also indicates that the leading correction to $f_+(0)$ in chiral perturbation theory (ChPT) does not contain the low-energy constants (LECs) of the next-leading order chiral Lagrangian, and hence is practically free of uncertainties.

In this paper, we calculate the vector form factor of the K_{l3} decay at zero momentum transfer $f_+(0)$ nonperturbatively from numerical simulations of lattice QCD with two degenerate flavors of dynamical quarks, which are identified with up and down quarks. Strange quarks are treated in the quenched approximation. To make the best of use of the good theoretical control mentioned in the previous paragraph, we employ a combination of the DBW2 gauge action [16] and the domain-wall quark action [17,18], which has excellent chiral symmetry even at finite lattice spacings. We also employ the so-called double ratio method [19] to improve the accuracy on the form factor. Preliminary results of these calculations have been reported in Ref. [20].

This paper is organized as follows. We present a brief introduction of the K_{l3} decays and status of experimental and theoretical studies on them in Sec. II. Our simulation method is introduced in Sec. III. Section IV is devoted to our determination of the form factor at finite momentum transfer from a double ratio of three-point functions. We describe the interpolation of the form factor to zero momentum transfer and the chiral extrapolation in Secs. V and VI. Section VII presents our estimate of $|V_{us}|$. Our conclusions are given in Sec. VIII.

II. K_{l3} DECAYS

A. Phenomenology of K_{l3} decays

The K_{l3} decays are K to π semileptonic decay channels

$$K^0_{l3}\colon K^0 \to \pi^- l^+ \nu_l, \tag{4}$$

$$K^+_{l3}\colon K^+ \to \pi^0 l^+ \nu_l, \tag{5}$$

where l represents the electron or muon. In the following, we mainly consider the neutral kaon decay K^0_{l3}. A simplification in theoretical studies of these decays is that the matrix element of the axial current vanishes due to the parity symmetry. Therefore, the decay amplitude contains only the matrix element of the vector current $V_\mu = \bar{s}\gamma_\mu u$ which can be expressed in terms of form factors

$$\langle \pi(p')|V_\mu|K(p)\rangle = (p_\mu + p'_\mu) f_+(q^2) + (p_\mu - p'_\mu) f_-(q^2), \tag{6}$$

where $q = p - p'$ represents the momentum transfer.

In literature, the so-called scalar form factor

$$f_0(q^2) = f_+(q^2) + \frac{q^2}{M_K^2 - M_\pi^2} f_-(q^2), \tag{7}$$

and

$$\xi(q^2) = \frac{f_-(q^2)}{f_+(q^2)} \tag{8}$$

are often used instead of $f_-(q^2)$. In particular, $f_0(q^2)$ is a useful quantity in lattice calculations, since i) it equals to $f_+(0)$, which appears in the expression of the decay rate (see Eq. (10) below), at zero momentum transfer $q^2 = 0$, ii) it can be precisely calculated from the matrix element with kaon and pion momenta equal to zero

$$\langle \pi(0)|V_4|K(0)\rangle = (M_K + M_\pi) f_0(q^2_{\max}), \tag{9}$$

where $q^2_{\max} = (M_K - M_\pi)^2$.

The rate of the K_{l3} decays is given by [15]

$$\Gamma = \frac{G_\mu^2}{192\pi^3} M_K^5 C^2 I |V_{us}|^2 |f_+(0)|^2 S_{\rm ew}(1 + \delta_{\rm em}), \tag{10}$$

where I and $S_{\rm ew}(1 + \delta_{\rm em})$ represent the phase space integral and radiative corrections, respectively. The Clebsch-Gordan coefficient $C^2 = 1(1/2)$ for the neutral (charged) kaon decay is written explicitly in the above expression so that $f_+(0)$ for both decay channels equals to unity in the $SU(3)$ symmetric limit.

The phase space integral I is generally defined as [15]

$$I = \frac{1}{M_K^8} \int d(q^2) \lambda_I^{3/2} \left(1 + \frac{M_l^2}{2q^2}\right)\left(1 - \frac{M_l^2}{q^2}\right)^2 \times \left\{\frac{f_+(q^2)}{f_+(q_0^2)} + \frac{3M_l^2 (M_K^2 - M_\pi^2)^2}{(2q^2 + M_l^2)\lambda_I} \frac{f_0(q^2)}{f_+(q_0^2)}\right\}, \tag{11}$$

$$\lambda_I = q^4 + M_K^4 + M_\pi^4 - 2q^2 M_K^2 - 2q^2 M_\pi^2 - 2M_K^2 M_\pi^2, \tag{12}$$

where q_0 is a reference value of the momentum transfer. If we take $q_0 \neq 0$, $f_+(0)$ in Eq. (10) has to be replaced by $f_+(q_0)$. As in Eq. (10), q_0 is usually set to 0 so that I depends on $f_{+,0}(q^2)$ only through small coefficients $\lambda_+^{(1)}$, $\lambda_+^{(2)}$ and $\lambda_0^{(1)}$, which parametrize the q^2 dependence of $f_{+,0}(q^2)$

$$f_+(q^2) = f_+(0)(1 + \lambda_+^{(1)} q^2 + \lambda_+^{(2)} q^4), \tag{13}$$

$$f_0(q^2) = f_0(0)(1 + \lambda_0^{(1)} q^2), \tag{14}$$

where we include the quadratic term suggested by the KTeV experiment to $f_+(q^2)$ [21]. From recent experimental measurements of these coefficients [21–23], the current estimate for I is ~0.154 (0.159) for K^0_{e3} (K^+_{e3}) and 0.102 for $K^0_{\mu 3}$ with an accuracy of around 1% [2,3], where a dominant error comes from the choice of the parametrization form of the q^2 dependence of $f_+(q^2)$. The choice of the reference scale $q_0 = 0$ forces us to study the q^2 dependence of the form factor and take the limit of $q^2 = 0$ as in Sec. V.

The radiative corrections split into the short-distance electroweak piece $S_{\rm ew}$ and the long-distance electromagnetic piece $(1 + \delta_{\rm em})$. The former is precisely determined as $S_{\rm ew} = 1.022$ [24]. Chiral perturbation theory including the electromagnetic interaction [25] and a phenomenological model [26] reveal that the latter is small correction, and its uncertainty leads to $\lesssim 1\%$ error to Γ.

Recently several new experimental determination of Γ have been performed to clarify the origin of the two σ deviation from unitarity in Eq. (3) [9–13]. In Ref. [3], $|V_{us} f_+(0)| = 0.2173$ is obtained from the new measurements of Γ and recent estimates of I and $\delta_{\rm em}$ through Eq. (10). This is about 3% larger than 0.2114 corresponding to $|V_{us}|$ in Eq. (2), and may lead to a good consistency with CKM unitarity. However, we have to determine $f_+(0)$ with an accuracy of 1% in order to make a definite conclusion on this unitarity test.

B. Previous theoretical studies of $f_+(0)$

In previous theoretical studies, $f_+(0)$ is considered in the following ChPT expansion

$$f_+(0) = 1 + f_2 + f_4 + O(p^6), \tag{15}$$

where f_{2n} is the $O(M^{2n}_{\pi,K,\eta}) = O(m_q^n)$ correction to $f_+(0)$. We note that the leading term is unity, because $f_+(0)$ becomes the Clebsch-Gordan coefficient in the $SU(3)$ symmetric limit thanks to the vector current conservation, and we explicitly factor it out Eq. (10).

The Ademollo-Gatto theorem [14] states that $SU(3)$ breaking effects are second order in $(m_s - m_{ud})$. From previous theoretical studies, it turned out that the $SU(3)$ breaking effects $f_+(0) - 1$ are order of 3–5%. Therefore, we can achieve 1% accuracy on $f_+(0)$ by calculating the $SU(3)$ breaking effects with an accuracy of 20%–30%, which is not prohibitively challenging.

In addition, the Ademollo-Gatto theorem guarantees that the leading correction f_2 does not contain any poorly-known LECs, which are associated with analytic terms from the $O(p^4)$ chiral Lagrangian. For example, its ChPT formula for the K^0_{l3} decay is given by [27]

$$f_2 = H_{K^0\pi} + \frac{1}{2} H_{K^+\pi} + \frac{3}{2} H_{K^+\eta} + \epsilon\sqrt{3}(H_{K\pi} - H_{K\eta}), \tag{16}$$

$$H_{PQ} = -\frac{1}{64\pi^2 f_\pi^2}\left\{M_P^2 + M_Q^2 + \frac{2M_P^2 M_Q^2}{M_P^2 - M_Q^2}\ln\left[\frac{M_Q^2}{M_P^2}\right]\right\}, \tag{17}$$

where $\epsilon = (\sqrt{3}/4)(m_d - m_u)/(m_s - m_{ud})$.

However, the next leading correction f_4 contains LECs in $O(p^4)$ and $O(p^6)$ chiral Lagrangians [28–32]. Therefore, f_4 is difficult to determine only from ChPT, and hence a phenomenological estimate $f_4 = -0.016(8)$ by Leutwyler and Roos [15] has been employed in previous determinations of $|V_{us}|$.

Clearly, it is desirable to calculate $f_+(0)$ nonperturbatively. This background led to the first lattice study in quenched QCD [33]. They demonstrated that lattice calculations can achieve the 1% accuracy for $f_+(0)$ by using a set of the so-called double ratios of correlation functions, and by making good use of the ChPT formula for f_2, namely, Eq. (16), in the chiral extrapolation of their lattice data. They employed the nonperturbatively $O(a)$-improved Wilson quark action and obtained $f_+(0) = 0.960(9)$, which is consistent with the Leutwyler-Roos's estimate.

The calculation was extended to two-flavor QCD with the $O(a)$-improved Wilson quark action [34] and to three-flavor QCD with an improved Kogut-Susskind (KS) quark action [35]. While the q^2 dependence of $f_+(q^2)$ has not been investigated in the latter study, their estimates of $f_+(0)$ are consistent with that in quenched QCD.

It is also worth while to note that the so-called twisted boundary condition [36], which enables us to explore small q^2 region, has been tested in quenched QCD [37].

III. SIMULATION METHOD

In this study, we calculate the kaon form factor $f_+(0)$ by numerical simulations of lattice QCD with two-flavors of dynamical quarks, which are identified with up and down quarks. We note that the isospin breaking effects in Eq. (16) is proportional to $\epsilon \approx 0.01$, and f_2 itself is of order 2%–3% shift, so the correction due to isospin breaking is well below our target accuracy on $f_+(0)$ of 1%. Strange quarks are treated in the quenched approximation. We employ the domain-wall quark action [17], which has the following advantages over the conventional Wilson- and KS-type actions.

First, it possesses chiral symmetry even at finite lattice spacings in the limit of $L_s \to \infty$, while the conventional Wilson- and KS-type fermions break the chiral symmetry explicitly. The chiral behavior of physical quantities may be distorted with the conventional fermions. Rigorously speaking, we have to take account of effects of the explicit symmetry breaking in the chiral extrapolation of the quantities obtained with the conventional fermions at finite lattice spacings [38,39]. In contrast, chiral extrapolations with domain-wall quarks are fairly straightforward and simple as they need use essentially continuum ChPT [40]. This is particularly important in this study of the K_{l3} from factor, since we can safely subtract the leading correction f_2 from our lattice data of $f_+(0)$ by using the ChPT formula Eq. (16) before the chiral extrapolation so that systematic uncertainties due to the extrapolation influence the final result only through the small higher order corrections.

Another advantage of the use of domain-wall quark action is that it is automatically $O(a)$-improved. Unlike the Wilson-type fermions, the nonperturbative tuning of

improvement coefficients for the vector current is not necessary to remove possibly large $O(a)$ effects [41]. We also note that the leading $O(a^2)$ scaling violation in physical quantities such as the kaon B parameter is not large at $a^{-1} \simeq 2$ GeV [42,43].

These virtues of domain-wall fermions are lost if L_s is not sufficiently large. Since the CPU cost is proportional to L_s, it is limited to values around 10–20 in practical unquenched simulations. In order to improve chiral properties of the form factors with L_s fixed, we employ the DBW2 gauge action [16] with which the light hadron spectrum and the kaon B parameter show better chiral properties than with the conventional plaquette action [44,45].

We use gauge ensembles generated on a $L^3 \times T = 16^3 \times 32$ lattice at $\beta = 0.80$, as discussed in Ref. [45]. The lattice spacing is $a \simeq 0.12$ fm and the physical spatial size is $La \simeq 1.9$ fm. We set the domain-wall height to $M_5 = 1.8$ and the fifth-dimensional length to $L_s = 12$. The resulting residual quark mass is a few MeV. We simulate sea quark masses $m_{ud,\mathrm{sea}} = 0.02$, 0.03, and 0.04 in the range of $m_{s,\mathrm{phys}}/2 \lesssim m_{ud,\mathrm{sea}} \lesssim m_{s,\mathrm{phys}}$, where $m_{s,\mathrm{phys}}$ represents the physical strange quark mass. Our statistics are 94 configurations separated by 50 HMC trajectories at each sea quark mass. We refer to Ref. [45] for further details on the configuration generation.

On these gauge ensembles, we calculate two and three point functions

$$C^P(t;\mathbf{p}) = \sum_{\mathbf{x}} \langle \mathcal{O}_{P,\mathrm{snk}}(\mathbf{x}, t+t_0)\mathcal{O}^\dagger_{P,\mathrm{src}}(\mathbf{0}, t_0)\rangle e^{-i\mathbf{p}\mathbf{x}}, \xrightarrow[t\to\infty]{} \frac{Z^*_{P,\mathrm{src}} Z_{P,\mathrm{snk}}}{2E_P(\mathbf{p})} e^{-E_P(\mathbf{p})t} \tag{18}$$

$$C^{PQ}_\mu(t,t';\mathbf{p},\mathbf{p}') = \sum_{\mathbf{x},\mathbf{x}'} \langle \mathcal{O}_{Q,\mathrm{snk}}(\mathbf{x}', t'+t_0) V_\mu(\mathbf{x}, t+t_0) \times \mathcal{O}^\dagger_{P,\mathrm{src}}(\mathbf{0}, t_0)\rangle e^{-i\mathbf{p}'(\mathbf{x}'-\mathbf{x})} e^{-i\mathbf{p}\mathbf{x}}, \xrightarrow[t,(t'-t)\to\infty]{} \frac{Z^*_{P,\mathrm{src}} Z_{Q,\mathrm{snk}}}{4E_P(\mathbf{p})E_Q(\mathbf{p}')Z_V} \times \langle Q(p')|V^{(\mathrm{R})}_\mu|P(p)\rangle e^{-E_P(\mathbf{p})t - E_Q(\mathbf{p}')(t'-t)} \tag{19}$$

where P and Q denote K or π meson. The sink (source) operator for the meson P is represented by $\mathcal{O}^{(\dagger)}_{P,\mathrm{snk(src)}}$, and its overlap to the physical meson state is given by $Z_{P,\mathrm{snk(src)}} = \langle 0|O_{P,\mathrm{snk(src)}}|P\rangle$. We denote the energy of meson P with a spatial momentum $\mathbf{p}$ by $E_P(\mathbf{p})$. The renormalized vector current with the renormalization factor Z_V is represented by $V^{(R)}_\mu$.

In our preliminary study [20], an exponential smeared operator

$$\sum_{\mathbf{r}} \phi(|\mathbf{r}|)\bar{q}(\mathbf{x})\gamma_5 q(\mathbf{x}+\mathbf{r}), \qquad \phi(|\mathbf{r}|) = A\exp[-B|\mathbf{r}|] \tag{20}$$

with $A = 1.2$ and $B = 0.1$ was used for the initial meson. We observe that the correlators $C^P(t;\mathbf{p})$ and $C^{PQ}_\mu(t,t';\mathbf{p},\mathbf{p}')$ with nonzero $\mathbf{p}$ show poor signals with this choice of the smearing function. This may suggest that this operator is too close to the wall source, and the correlators have small overlap with meson states with nonzero $\mathbf{p}$. In this study, therefore, we use more localized operators with $B = 0.5$, 0.6, and 0.7 at $m_{ud} = 0.02$, 0.03, and 0.04, respectively. We take a single choice of $t_0 = 4$ for both of $C^P(t;\mathbf{p})$ $C^{PQ}_\mu(t,t';\mathbf{p},\mathbf{p}')$. The local operator, which is combined with the sequential source method [46] for $C^{PQ}_\mu(t,t';\mathbf{p},\mathbf{p}')$, is used for the sink meson operator.

As in Ref. [45], we calculate the quark propagator with each of the periodic and antiperiodic boundary conditions in temporal direction for quarks. The correlation functions C^P and C^{PQ}_μ are constructed by using the averaged quark propagator over the boundary conditions. This procedure cancels effects of valence quarks wrapping the lattice in the temporal direction by odd number of times, and enable us to take the time slice for the sink operator $(t' + t_0)$ for C^{PQ}_μ larger than $T/2$. In this study, we fix t' to 24 for all combinations of sea and valence quark masses.

In our measurement of C^P and C^{PQ}_μ, we fix the valence ud quark mass equal to the sea quark mass, and take four strange quark masses $m_s = 0.02$, 0.03, 0.04, and 0.05, which are roughly in a range of $[m_{s,\mathrm{phys}}/2, 5m_{s,\mathrm{phys}}/4]$. For the meson momentum, we take all possible configurations $\mathbf{p}$ with $|\mathbf{p}|^2 = 0$, 1, and 2 for the initial meson "P" in C^P and C^{PQ}_μ. For notational simplicity, we use the momentum p_k in units of $2\pi/L_k$ throughout this paper. Two configurations $\mathbf{p} = (0,0,0)$ and $(-1,0,0)$ are used for the final meson "Q" in C^{PQ}_μ.

IV. SCALAR FORM FACTOR AT q^2_{max}

A. Meson masses

In extraction of the form factors from C^{PQ}_μ, we need precise knowledge of the pion and kaon masses and their energies with finite momenta, which appear in Eq. (19). In Fig. 1, we plot the effective mass for pions calculated from C^π. We observe a clear and long plateau in the effective mass, and hence the (lattice) meson masses summarized in Table I are determined with an accuracy of $\lesssim 1\%$. We note that masses presented in Ref. [45], in which the local and wall sources are employed, are consistent with ours within statistical error.

For the meson energies with nonzero momenta, we use an estimation from the fitted mass M and the lattice dispersion relation

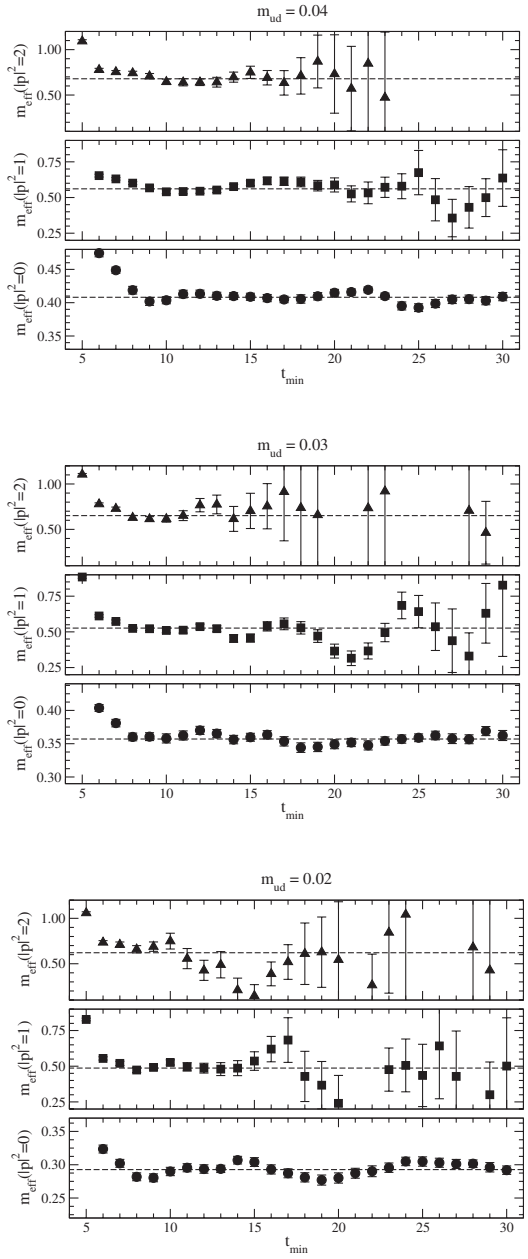

FIG. 1. Effective mass plots for pion at $m_{ud} = 0.04$ (top figure), 0.03 (middle figure), and 0.02 (bottom figure). Lines for data with zero meson momentum represent the fitted mass, while those for larger momentum are an estimation from the lattice dispersion relation Eq. (21).

$$\hat{E}(\mathbf{p})^2 = M^2 + \hat{\mathbf{p}}^2, \qquad \hat{E}(\mathbf{p}) = 2\sinh\left[\frac{E(\mathbf{p})}{2}\right], \qquad p_k = 2\sin\left[\frac{p_k}{2}\right], \tag{21}$$

instead of the fitted energy to C^P, since its statistical error rapidly increases as the size of the meson momentum increases. We observe that i) the fitted energy shows a good consistency with Eq. (21) as in Fig. 2; ii) the final result for $f_+(0)$ at the physical quark mass does not change significantly if we use the dispersion relation in the continuum limit instead of Eq. (21).

B. $f_0(q^2_{\mathrm{max}})$

We consider the double ratio which was originally proposed in Ref. [19] for B meson decays

$$R(t) = \frac{C_4^{K\pi}(t, t'; \mathbf{0}, \mathbf{0}) C_4^{\pi K}(t, t'; \mathbf{0}, \mathbf{0})}{C_4^{KK}(t, t'; \mathbf{0}, \mathbf{0}) C_4^{\pi\pi}(t, t'; \mathbf{0}, \mathbf{0})}, \tag{22}$$

where we fix t' to 24 as mentioned in Sec. III, and t' dependence of R is ignored in the following. All of Z_V, $Z_{P,\mathrm{src}}$, $Z_{Q,\mathrm{snk}}$ and the exponential damping factor in Eq. (19) are exactly canceled in $R(t)$. As a result, $R(t)$ contains only meson matrix elements with zero momentum, and gives $f_0(q^2_{\mathrm{max}})$

$$R(t) \underset{t,(t'-t)\to\infty}{\longrightarrow} \frac{\langle\pi|V_4^{(\mathrm{R})}|K\rangle\langle K|V_4^{(\mathrm{R})}|\pi\rangle}{\langle K|V_4^{(\mathrm{R})}|K\rangle\langle\pi|V_4^{(\mathrm{R})}|\pi\rangle} = \frac{(M_K + M_\pi)^2}{4M_K M_\pi}|f_0(q^2_{\mathrm{max}})|^2. \tag{23}$$

We note that $R(t)$ is exactly equal to unity in the $SU(3)$ symmetric limit and hence it is a useful quantity to measure $SU(3)$ breaking effects to $f_0(q^2_{\mathrm{max}})$.

In Fig. 3, we show the three-point functions $C_4^{K\pi}$, $C_4^{\pi K}$, C_4^{KK} and $C_4^{\pi\pi}$ for each jackknife sample. Their fluctuation leads to the jackknife error of about 5%. As seen in the figure, they are highly correlated with each other, and hence the double ratio $R(t)$ has a very small fluctuation over the jackknife samples, which leads to the error of about 0.03%.

TABLE I. Fitted meson masses.

m_{ud}		M_π	m_{ud}		M_π	m_{ud}		M_π
0.02		0.2927(18)	0.03		0.3570(26)	0.04		0.4081(21)
m_{ud}	m_s	M_K	m_{ud}	m_s	M_K	m_{ud}	m_s	M_K
0.02	0.03	0.3239(17)	0.03	0.02	0.3288(28)	0.04	0.02	0.3565(22)
0.02	0.04	0.3528(17)	0.03	0.04	0.3836(24)	0.04	0.03	0.3830(20)
0.02	0.05	0.3797(17)	0.03	0.05	0.4088(24)	0.04	0.05	0.4323(21)

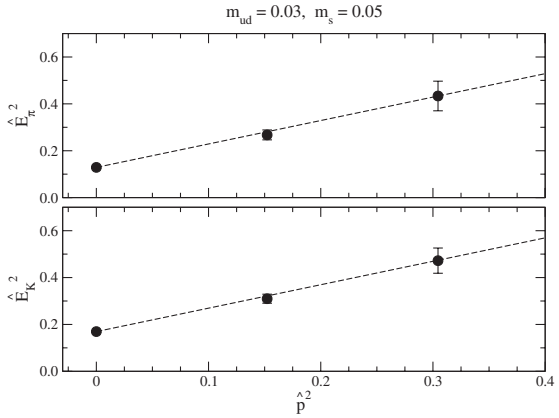

FIG. 2. Comparison of fitted energies (circles) with lattice dispersion relation Eq. (21) at $(m_{ud}, m_s) = (0.03, 0.05)$. Top and bottom panels show pion and kaon energies, respectively.

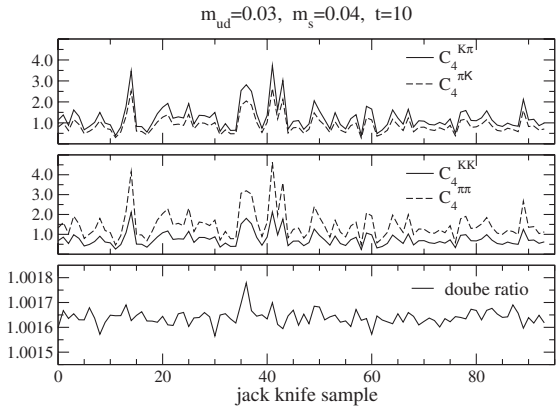

FIG. 3. Three-point functions (top and middle panels) and their double ratio R for each jackknife sample at $(m_{ud}, m_s) = (0.03, 0.04)$.

Figure 4 shows that the magnitude of the statistical error does not change drastically at other values of t. From the fitted value of $R(t)$ and measured meson masses on lattice, we obtain $f_0(q^2_{\max})$ summarized in Table II. There is a tendency that the error of $f_0(q^2_{\max})$ increases as m_s deviates from m_{ud}, which is probably because $f_0(q^2_{\max})$ deviates from its trivial value 1 towards larger $|m_s - m_{ud}|$. However, the statistical accuracy is $\lesssim 0.1\%$ even in the worst case $(m_{ud}, m_s) = (0.02, 0.05)$.

V. INTERPOLATION TO ZERO MOMENTUM TRANSFER

To study the q^2 dependence of the form factor, we calculate

$$F(\mathbf{p}, \mathbf{p}') = \frac{f_+(q^2)}{f_0(q^2_{\max})}\left(1 + \frac{E_K(\mathbf{p}) - E_\pi(\mathbf{p}')}{E_K(\mathbf{p}) + E_\pi(\mathbf{p}')}\xi(q^2)\right), \quad (24)$$

from a ratio

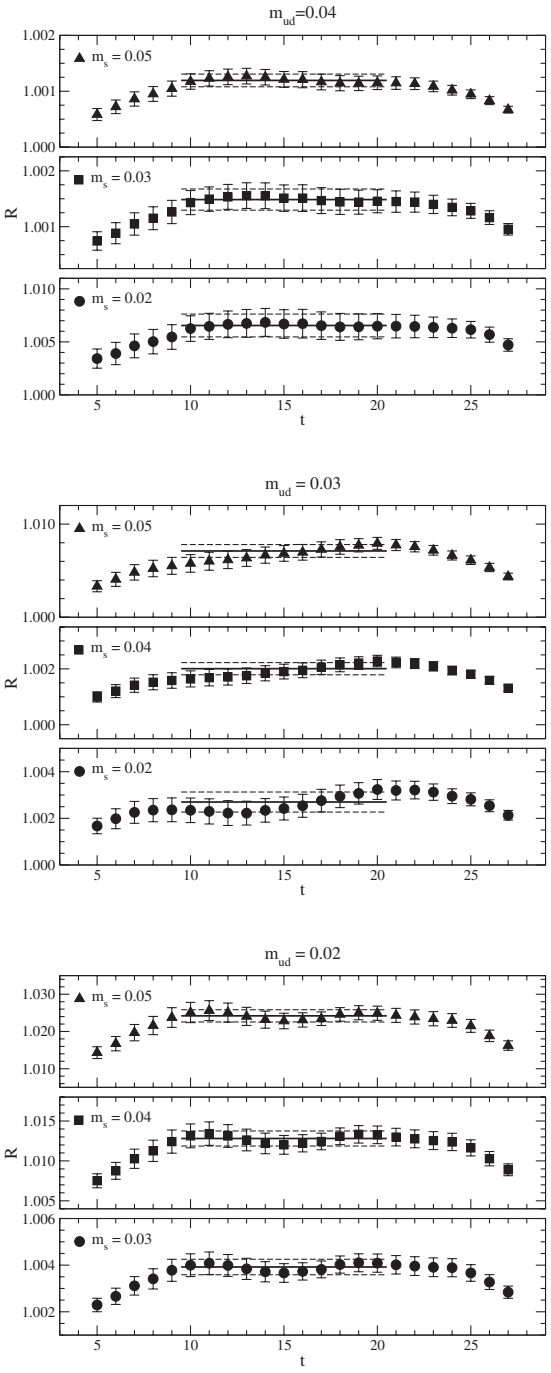

FIG. 4. Double ratio Eq. (22) at $m_{ud} = 0.04$ (top figure), 0.03 (middle figure), and 0.02 (bottom figure).

$$\tilde{R}(t; \mathbf{p}, \mathbf{p}') = \frac{C_4^{K\pi}(t, t'; \mathbf{p}, \mathbf{p}')C^K(t; \mathbf{0})C^\pi(t' - t; \mathbf{0})}{C_4^{K\pi}(t, t'; \mathbf{0}, \mathbf{0})C^K(t; \mathbf{p})C^\pi(t' - t; \mathbf{p}')} \xrightarrow[t,(t'-t)\to\infty]{} \frac{E_K(\mathbf{p}) + E_\pi(\mathbf{p}')}{M_K + M_\pi} F(\mathbf{p}, \mathbf{p}'). \quad (25)$$

Since $\tilde{R}(t; \mathbf{p}, \mathbf{p}')$ has its trivial value 1 at $|\mathbf{p}| = |\mathbf{p}'| = 0$, it might be a good probe to study how $f_0(q^2)$ changes as q^2

TABLE II. Scalar form factor $f_0(q^2_{\rm max})$ at simulated quark masses.

m_{ud}	m_s	$f_0(q^2_{\rm max})$	m_{ud}	m_s	$f_0(q^2_{\rm max})$	m_{ud}	m_s	$f_0(q^2_{\rm max})$
0.02	0.03	1.000 67(17)	0.03	0.02	1.000 50(22)	0.04	0.02	1.000 98(55)
0.02	0.04	1.002 02(48)	0.03	0.04	1.000 36(11)	0.04	0.03	1.000 24(10)
0.02	0.05	1.003 52(82)	0.03	0.05	1.001 26(35)	0.04	0.05	1.000 18(6)

deviates from $q^2_{\rm max}$. We also note that $\tilde{R}(t;\mathbf{p},\mathbf{p}')$ is reduced to the double ratio employed in Ref. [34], if we fix $\mathbf{p}=\mathbf{0}$.

In order to reduce the statistical error, we calculate $\tilde{R}(t;\mathbf{p},\mathbf{p}')$ from three-point functions averaged over momentum configurations which correspond to the same momentum sizes $|\mathbf{p}|$ and $|\mathbf{p}'|$. Figure 5 shows example of $F(\mathbf{p},\mathbf{p}')$ obtained from $\tilde{R}(t;\mathbf{p},\mathbf{p}')$ as a function of t. We observe that data with the smallest nonzero momentum $|\mathbf{p}|^2=1$ show a clear plateau, and hence $F(\mathbf{p},\mathbf{p}')$ is determined with an accuracy of roughly 5%.

In order to convert $F(\mathbf{p},\mathbf{p}')$ to $f_0(q^2)$, we evaluate $\xi(q^2)$ by employing the method proposed in Ref. [33]. Namely, we measure the double ratio

$$R_k(t;\mathbf{p},\mathbf{p}')=\frac{C_k^{K\pi}(t,t';\mathbf{p},\mathbf{p}')C_4^{KK}(t,t';\mathbf{p},\mathbf{p}')}{C_4^{K\pi}(t,t';\mathbf{p},\mathbf{p}')C_k^{KK}(t,t';\mathbf{p},\mathbf{p}')},\qquad (k=1,2,3), \tag{26}$$

and calculate $\xi(q^2)$ from

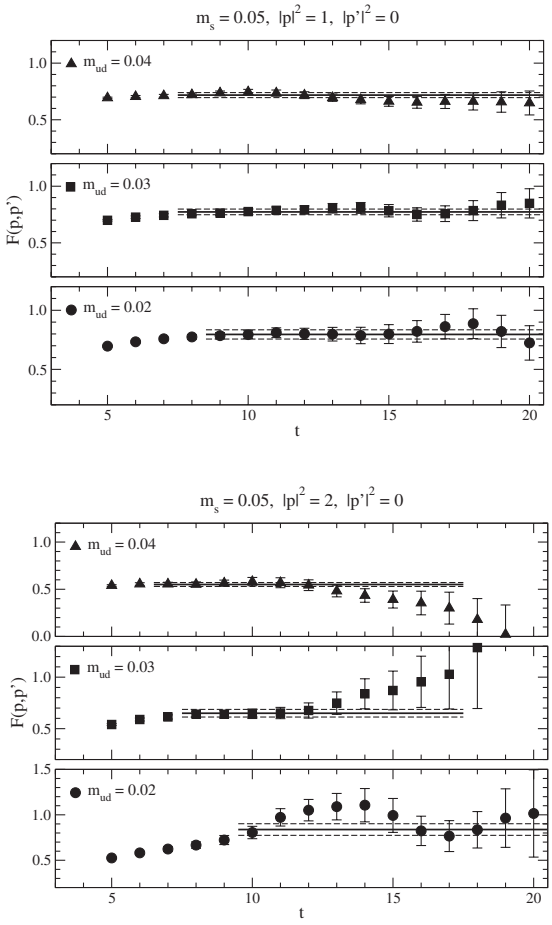

FIG. 5. Plots of $F(\mathbf{p},\mathbf{p}')$ defined by Eq. (24) with $m_s=0.05$ and $|\mathbf{p}'|=0$. Top and bottom figures show data with $|\mathbf{p}|^2=1$ and 2, respectively.

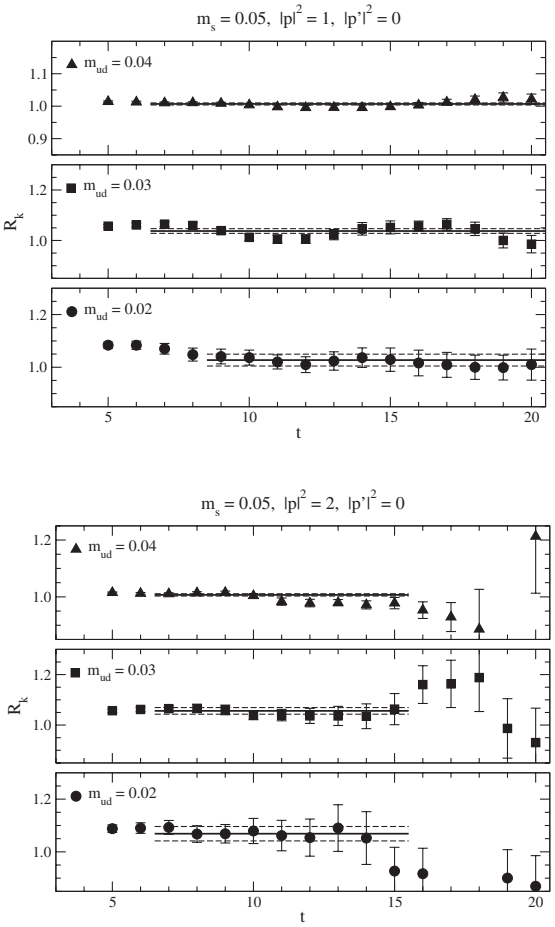

FIG. 6. Plots of double ratio $R_k(t;\mathbf{p},\mathbf{p}')$ defined by Eq. (26) with $m_s=0.04$ and $|\mathbf{p}'|=0$. Top and bottom figures show data with $|\mathbf{p}|^2=1$ and 2, respectively.

$$\xi(q^2) = \frac{-(E_K(\mathbf{p}) + E_K(\mathbf{p}'))(p + p')_k + (E_K(\mathbf{p}) + E_\pi(\mathbf{p}'))(p + p')_k R_k}{(E_K(\mathbf{p}) + E_K(\mathbf{p}'))(p - p')_k - (E_K(\mathbf{p}) - E_\pi(\mathbf{p}'))(p + p')_k R_k}. \quad (27)$$

As for $\tilde{R}(t; \mathbf{p}, \mathbf{p}')$, we first take the average for the relevant three-point functions over appropriately chosen momentum configuration and the Lorentz index for V_μ ($\mu = 1, 2, 3$), and then double ratio $R_k(t; \mathbf{p}, \mathbf{p}')$ is constructed from the averaged correlation function. We note that $R_k(t; \mathbf{p}, \mathbf{p}')$ is exactly unity in the $SU(3)$ symmetric limit, and is sensitive to $SU(3)$ breaking effects in the matrix element $C_\mu^{K\pi}$.

Figure 6 shows examples of $R_k(t; \mathbf{p}, \mathbf{p}')$ as a function of t. We observe that, at most of our simulated quark masses, $R_k(t; \mathbf{p}, \mathbf{p}')$ is close to unity, and hence $\xi(q^2)$ from Eq. (27) has small magnitude $\lesssim 0.1$. Its error is typically 30%–100% with our statistics.

We note that $F(\mathbf{p}, \mathbf{p}')$ and $\xi(q^2)$ can be calculated also from the following ratios constructed from the $\pi \to K$ matrix element

$$\tilde{R}'(t; \mathbf{p}, \mathbf{p}') = \frac{C_4^{\pi K}(t, t'; \mathbf{p}, \mathbf{p}') C^\pi(t; \mathbf{0}) C^K(t' - t; \mathbf{0})}{C_4^{\pi K}(t, t'; \mathbf{0}, \mathbf{0}) C^\pi(t; \mathbf{p}) C^K(t' - t; \mathbf{p}')}, \quad (28)$$

$$R_k'(t; \mathbf{p}, \mathbf{p}') = \frac{C_k^{\pi K}(t, t'; \mathbf{p}, \mathbf{p}') C_4^{KK}(t, t'; \mathbf{p}, \mathbf{p}')}{C_4^{\pi K}(t, t'; \mathbf{p}, \mathbf{p}') C_k^{KK}(t, t'; \mathbf{p}, \mathbf{p}')}. \quad (29)$$

We confirm that, for $|\mathbf{p}| = 0$ and $|\mathbf{p}'| = 1$, $\tilde{R}(t; \mathbf{p}, \mathbf{p}')$ and $\tilde{R}'(t; \mathbf{p}', \mathbf{p})$ give consistent results for $F(\mathbf{p}, \mathbf{p}')$, while the latter leads to much smaller error. This is because, as described in Sec. III, $C_\mu^{PQ}(t, t'; \mathbf{p}, \mathbf{p}')$ is measured with the single choice of the final meson momentum $\mathbf{p}'$ for each $|\mathbf{p}'|$, and we can not take average of $\tilde{R}(t; \mathbf{p}, \mathbf{p}')$ over the momentum configuration "$\{\mathbf{p}'\}$". We also observe that data with $|\mathbf{p}|$, $|\mathbf{p}'| > 0$ show poor signal. Therefore, in the following analysis, we use $F(\mathbf{p}, \mathbf{p}')$ and $\xi(q^2)$ obtained from $\tilde{R}(t; \mathbf{p}, \mathbf{p}')$, $R_k(t; \mathbf{p}, \mathbf{p}')$, $\tilde{R}'(t; \mathbf{p}, \mathbf{p}')$, and $R_k'(t; \mathbf{p}, \mathbf{p}')$ with $|\mathbf{p}'| = 0$.

In order to take the limit of zero momentum transfer of $f_0(q^2)$ reliably, we test two methods to calculate $f_0(0)$, and check the consistency between results from these methods. In the first method, which we call method-1 in the following, we calculate $f_0(q^2)$ at simulated q^2 from $F(\mathbf{p}, \mathbf{p}')$ and $\xi(q^2)$. Then, the results for $f_0(q^2)$ and $f_0(q^2_{\rm max})$ from $R(t)$ are interpolated to $q^2 = 0$. As well as the linear fitting form Eq. (14), we test the quadratic form

$$f_0(q^2) = f_0(0)(1 + \lambda_0^{(1)} q^2 + \lambda_0^{(2)} q^4), \quad (30)$$

and the pole form

$$f_0(q^2) = f_0(0)/(1 - \lambda_0^{(1)} q^2). \quad (31)$$

The physical value of $q^2_{\rm max}$ for K_{l3} decays is much smaller than that for B meson decays. In addition, $q^2_{\rm max}$ is further reduced in our lattice calculation, since the simulated values of m_{ud} are larger than its physical value. As shown in Fig. 7, $f_0(0)$ can be determined by a very short

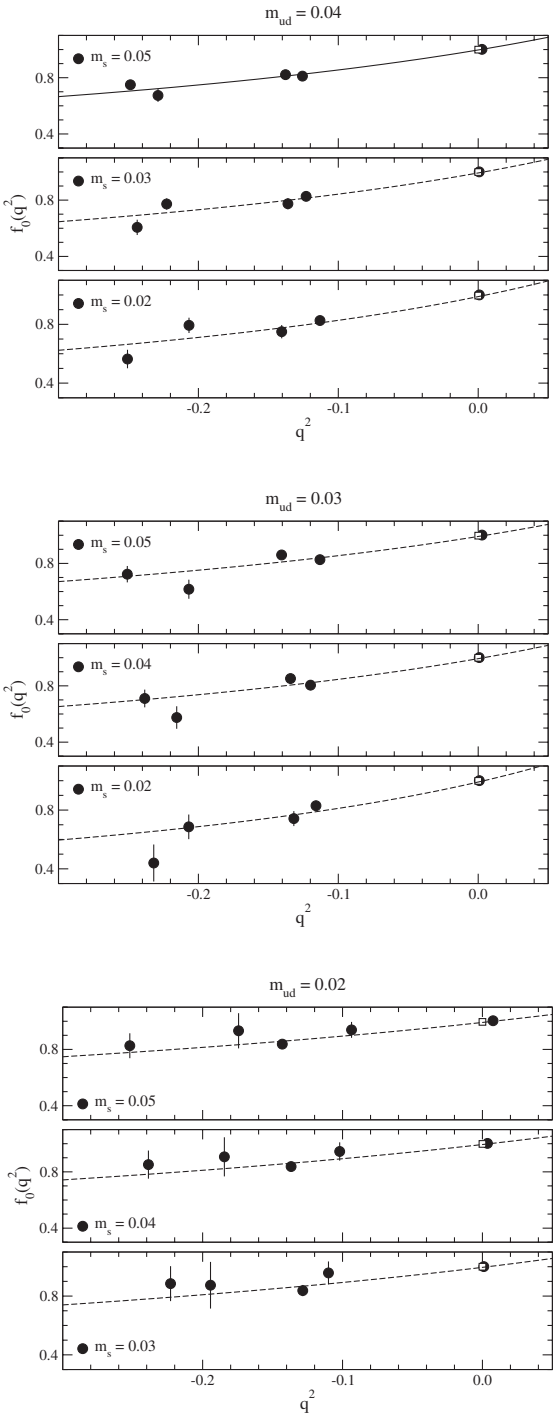

FIG. 7. Pole model interpolation of $f_0(q^2)$ to $q^2 = 0$. Top, middle and bottom figures show results at sea quark mass $m_{ud} = 0.04$, 0.03 and 0.02, respectively. Filled circles are $f_0(q^2)$ at simulated q^2, while open squares represent interpolated value to $q^2 = 0$.

interpolation from $q^2_{\rm max}$, where we have very accurate data $f_0(q^2_{\rm max})$ from $R(t)$. As a result, the choice of the interpolation form does not affect the interpolated value $f_0(0)$ significantly. Actually we observe that the interpolated values obtained from the three forms, Eqs. (14), (30), and (31) are consistent with each other.

In the following, we employ the result from the pole form Eq. (31), because i) data of $f_0(q^2)$ does not have a strong curvature, and hence the quadratic fit leads to ill-determined $\lambda_0^{(2)}$, which has typically 100% error, and ii) the pole form leads to slightly smaller value of χ^2/dof than the linear fit. The fit parameters are summarized in Table III. While the pole form at $m_{ud} = 0.03$ leads to a slightly higher value of χ^2/dof than at other values of m_{ud}, the inclusion of the quadratic term does not reduce χ^2/dof significantly. We note that the statistical error on $f_0(0)$ is $\lesssim 0.3\%$ level.

We also test an alternative method to calculate $f_0(0)$ employed in Ref. [34], which we call method-2 in the following. In this method, we first take the limit of $F(\mathbf{p}, \mathbf{p}')$ and $\xi(q^2)$ to $q^2 = 0$, and then calculate $f_0(0)$ from $F(\mathbf{p}, \mathbf{p}')|_{q^2=0}$ and $\xi(0)$. Since $F(\mathbf{p}, \mathbf{p}')$ depends on two momenta $|\mathbf{p}|$, and $|\mathbf{p}'|$, the q^2 interpolation of $F(\mathbf{p}, \mathbf{p}')$ has to be carried out using data with fixed $|\mathbf{p}|$ (or $|\mathbf{p}'|$). This also enables us to identify $|\mathbf{p}'|$ ($|\mathbf{p}|$) corresponding to $q^2 = 0$, which is needed to convert $F(\mathbf{p}, \mathbf{p}')|_{q^2=0}$ to $f_0(0)$. In the following, we repeat the interpolation for two data sets with $|\mathbf{p}| = 0$ and $|\mathbf{p}'| = 0$, and take the average of results for $F(\mathbf{p}, \mathbf{p}')|_{q^2=0}$.

For the q^2 interpolation, we test linear, pole, and quadratic fitting forms similar to Eqs. (14), (30), and (31), and employ the quadratic fit

$$F(\mathbf{p}, \mathbf{p}')|_{q^2} = F(\mathbf{p}, \mathbf{p}')|_{q^2=0} \cdot (1 + c_{F,1} q^2 + c_{F,2} q^4) \quad (|\mathbf{p}| \text{ or } |\mathbf{p}|' \text{ is fixed}), \tag{32}$$

since this fit leads to the smallest value for χ^2/dof among the tested forms, and to the reasonably well-determined $c_{F,2}$. Examples of this quadratic fit are shown in Fig. 8.

While $\xi(0)$ has to be determined by an extrapolation, we observe that $\xi(q^2)$ has very mild q^2 dependence, as seen in Fig. 9, and the simplest linear form

$$\xi(q^2) = \xi(0)(1 + c_{\xi,1} q^2) \tag{33}$$

leads to reasonably small χ^2/dof. Table IV shows $\xi(0)$ and $f_0(0)$ calculated from $F(\mathbf{p}, \mathbf{p}')|_{q^2=0}$ and $\xi(0)$.

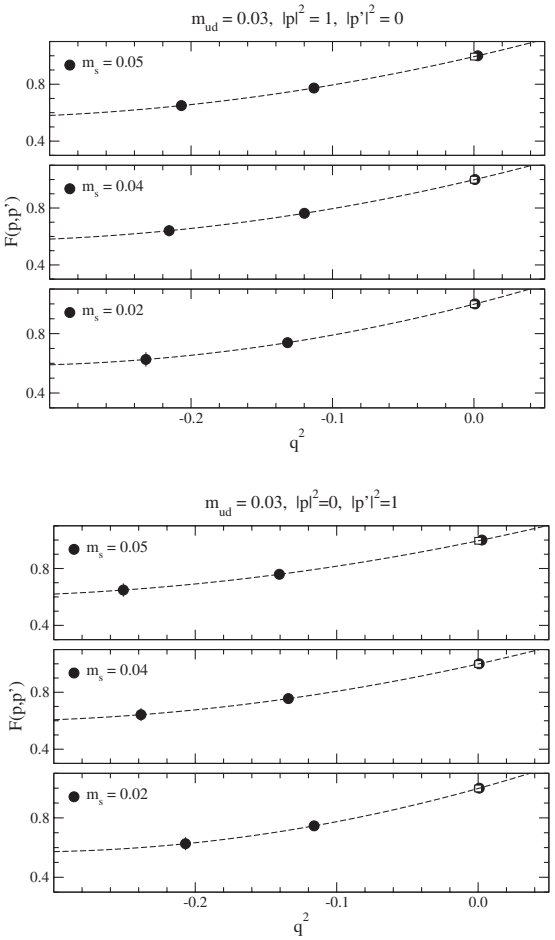

FIG. 8. Interpolation of $F(\mathbf{p}, \mathbf{p}')$ as a function of q^2 at $m_{ud} = 0.03$. Top and bottom figures show data with $|\mathbf{p}'| = 0$ and $|\mathbf{p}| = 0$, respectively.

TABLE III. Fit parameters for interpolation of $f_0(q^2)$ to $q^2 = 0$ using pole form Eq. (31).

m_{ud}	m_s	χ^2/dof	$f_0(0)$	$\lambda_0^{(1)}$
0.02	0.03	0.76	0.999 55(47)	1.16(39)
0.02	0.04	0.67	0.997 9(14)	1.13(32)
0.02	0.05	0.60	0.995 2(25)	1.09(28)
0.03	0.02	1.49	0.998 72(43)	2.23(40)
0.03	0.04	1.91	0.999 12(26)	1.75(32)
0.03	0.05	2.07	0.996 97(90)	1.60(30)
0.04	0.02	1.98	0.995 74(95)	1.97(33)
0.04	0.03	1.79	0.999 11(20)	1.80(28)
0.04	0.05	1.06	0.999 24(15)	1.61(23)

TABLE IV. Results for $\xi(0)$ and $f_0(0)$ obtained from Eqs. (32) and (33).

m_{ud}	m_s	$\xi(0)$	$f_0(0)$
0.02	0.03	−0.056(23)	1.000 07(94)
0.02	0.04	−0.101(34)	0.999 2(29)
0.02	0.05	−0.133(39)	0.996 2(57)
0.03	0.02	+0.041(15)	1.000 17(58)
0.03	0.04	−0.0307(94)	0.999 85(36)
0.03	0.05	−0.053(16)	0.999 0(12)
0.04	0.02	+0.050(22)	0.996 8(15)
0.04	0.03	+0.0195(85)	0.999 15(31)
0.04	0.05	−0.0144(65)	0.999 12(24)

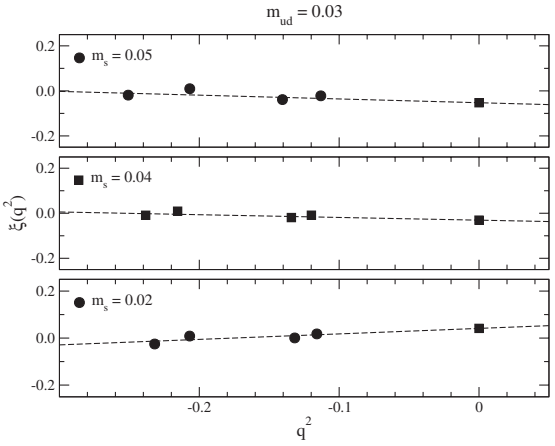

FIG. 9. Linear extrapolation of $\xi(q^2)$ as a function of q^2 at $m_{ud} = 0.03$.

We observe that two methods of the q^2 interpolation give consistent results for $f_0(0)$ with each other. However, the error from method-2 is slightly larger than from method-1 due to the error for $\xi(0)$ enhanced by the extrapolation. Therefore, we employ results from method-1 in the following.

We note that the above observation is opposite from that in our preliminary study [20], where method-1 give larger error for $f_0(0)$ mainly due to the uncertainty in $\xi(q^2)$ at simulated q^2. As described in Sec. III, we calculate correlation functions with the different choice of the smearing function from that in Ref. [20]. This improves accuracy in $\xi(q^2)$ at simulated q^2 and hence $f_0(0)$ in method-1. However, in order to reduce the uncertainty from method-2, the change of the smearing functions is not sufficient and we need to have data at small q^2 for a better control of the extrapolation of $\xi(q^2)$.

VI. CHIRAL EXTRAPOLATION

In the chiral extrapolation of $f_+(0) = f_0(0)$, we rewrite the ChPT expansion Eq. (15) as

$$f_+(0) = 1 + f_2 + \Delta f, \tag{34}$$

where Δf represents all higher order corrections starting at $O(M^4_{K,\pi,\eta})$.

As mentioned in Sec. II, the leading correction f_2 does not have analytic terms from the $O(p^4)$ chiral Lagrangian thanks to the Ademollo-Gatto theorem. It is shown in Ref. [47] that the above statement is true even in two-flavor partially quenched (PQ) theory, as seen in their PQChPT formula of f_2

$$f_2^{(\mathrm{PQ})} = -\frac{2M_K^2 + M_\pi^2}{32\pi^2 f_\pi^2} - \frac{3M_K^2 M_\pi^2 \ln[M_\pi^2/M_K^2]}{64\pi^2 f_\pi^2 (M_K^2 - M_\pi^2)} + \frac{M_K^2(4M_K^2 - M_\pi^2)\ln[2 - M_\pi^2/M_K^2]}{64\pi^2 f_\pi^2 (M_K^2 - M_\pi^2)}. \tag{35}$$

Therefore, f_2 does not contain any poorly-known LECs in the $O(p^4)$ chiral Lagrangian, and its value at simulated quark mass can be precisely calculated from the measured meson masses through Eq. (35).

Consequently, the chiral extrapolation of $f_+(0)$ is nothing but the extrapolation of the higher order correction Δf. Since it is also proportional to $(m_s - m_{ud})^2$ thanks to the Ademollo-Gatto theorem, we consider the ratio

$$R_{\Delta f} = \frac{\Delta f}{(M_K^2 - M_\pi^2)^2}, \tag{36}$$

as in Ref. [33], and extrapolate it to the physical quark mass. To this end, we test the following constant, linear and quadratic fits

$$R_{\Delta f} = c_0, \tag{37}$$

$$R_{\Delta f} = c_0 + c_{1,v}(M_K^2 + M_\pi^2), \tag{38}$$

$$R_{\Delta f} = c_0 + c_{1,s}M_\pi^2 + c_{1,v}(M_K^2 + M_\pi^2), \tag{39}$$

$$R_{\Delta f} = c_0 + c_{1,s}M_\pi^2 + c_{1,v}(M_K^2 + M_\pi^2) + c_{2,s}M_\pi^4 + c_{2,v}(M_K^2 + M_\pi^2)^2. \tag{40}$$

The constant fit Eq. (37) should work if Δf is dominated by

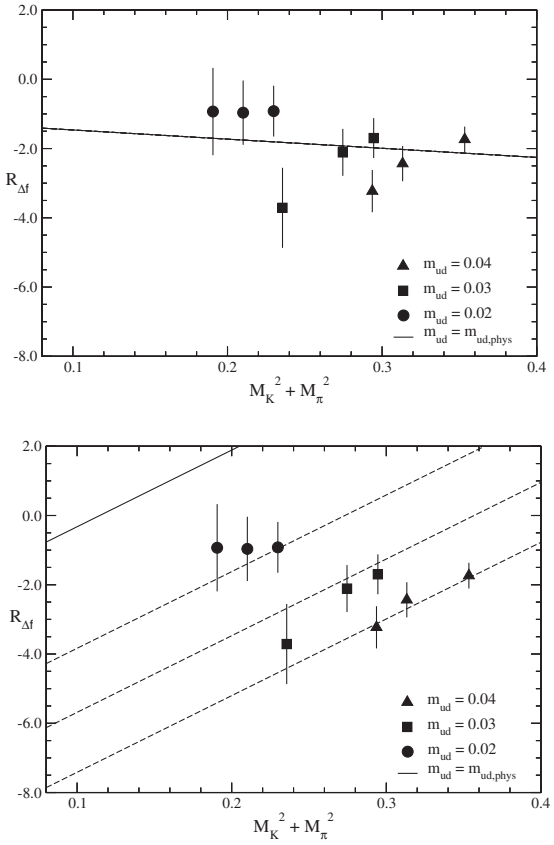

FIG. 10. Chiral extrapolation of $R_{\Delta f}$. Top and bottom figures show results using Eqs. (38) and (39), respectively.

TABLE V. Fit parameters for chiral extrapolation of $f_+(0)$, and Δf at physical quark mass.

fit form	χ^2/dof	c_0	$c_{1,s}$	$c_{1,v}$	Δf
Equation (37)	0.46	−1.99(34)	...	...	−0.013(2)
Equation (38)	0.46	−1.2(2.0)	...	−2.6(6.3)	−0.009(9)
Equation (39)	0.10	−2.3(1.8)	−44(14)	22.1(5.4)	−0.003(11)

the analytic term in f_4. Linear and quadratic dependences in Eqs. (38)–(40) are assumptions for an effective description of the chiral logarithms in f_4 and higher order corrections.

Figure 10 shows the chiral extrapolation using the linear forms Eqs. (38) and (39). We observe that $R_{\Delta f}$ has mild dependence on the sea and valence quark masses, and the linear and even constant fits achieve sufficiently small value of χ^2/dof. While the quadratic fit Eq. (40) also gives a small value of χ/dof, it leads to more than 100% error for both of $c_{2,s}$ and $c_{2,v}$. We, therefore, do not use the results from the quadratic fit in the following discussion.

From the fit parameters summarized in Table V and the physical meson masses determined in Ref. [45], we obtain Δf at the physical quark mass which is also collected in Table V. We note that all fits lead to consistent results for Δf with each other. We obtain

$$\Delta f = -0.009(9)(6), \tag{41}$$

by employing result from the linear fit Eq. (39), which is also employed in the unquenched calculations in Refs. [34,35]. The first error is statistical, and the second is a systematic error due to the chiral extrapolation which is estimated as the largest deviation in Δf among the constant and linear fits.

By using $f_2 = -0.023$ at physical quark mass in full QCD, we obtain

$$f_+(0) = 0.968(9)(6), \tag{42}$$

which is consistent with the previous lattice calculations [33–35], employing different discretizations (Wilson and KS) in quenched and unquenched QCD, listed in Table VI, as well as with estimates based on $O(p^6)$ ChPT [30–32], and the Leutwyler-Roos's value [15].

In Eq. (42), we have not included systematic uncertainties due to the discretization error and effects of dynamical strange quarks, which are difficult to estimate reliably without simulations at different lattice spacings or those in three-flavor QCD. However, these uncertainties affect our estimate of $f_+(0)$ only through the small higher order correction Δf, and hence are expected not to be large. This is supported by the nice consistency with results from different lattice actions and/or with different numbers of flavors for dynamical quarks (see Table VI). We also note that the RBC and UKQCD Collaborations have already started large-scale simulations with three flavors of dynamical domain-wall quarks, and their preliminary estimate is consistent with Eq. (42). In particular, that comparison should provide a more reliable estimate of systematic error due to quenching of strange quarks.

We also calculate $\xi(0)$ at the physical quark mass. Since $\xi(0)$ vanishes in the $SU(3)$ symmetric limit, we test the following simple linear fit

$$\xi(0) = d_{1,v}(M_K^2 - M_\pi^2), \tag{43}$$

and find that this leads to a reasonable value of χ^2/dof as shown in Table VII. The fit line is plotted in Fig. 11. We obtain

$$\xi(0) = -0.105(22), \tag{44}$$

which is consistent with the experimental values −0.01(6) for K^0_{l3} and −0.125(23) for K^+_{l3} [4].

TABLE VI. Recent lattice estimates of $f_+(0)$. Note that unquenched results in Ref. [34,35] are preliminary. Two values in Ref. [34] are obtained from two choices of the chiral extrapolation form (polynomial and ChPT based forms).

	N_f	quark action	$f_+(0)$
this work	2	domain-wall	0.968(11)
Becirevic *et al.* [33]	0	improved Wilson	0.960(9)
JLQCD [34]	2	improved Wilson	0.967(6), 0.952(6)
MILC [35]	3	improved staggered	0.962(11)

TABLE VII. Fit parameter for chiral extrapolation of $\xi(0)$.

χ^2/dof	$d_{1,v}$
0.45	−1.30(28)

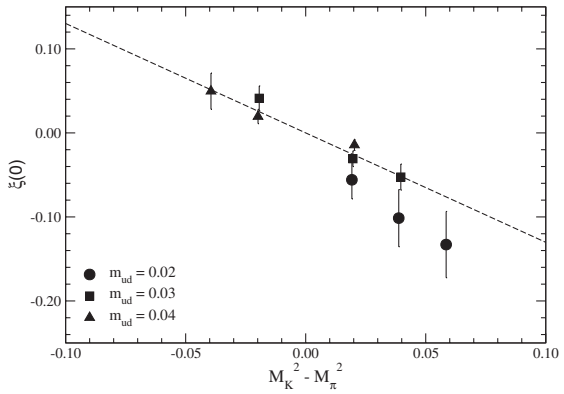

FIG. 11. Chiral extrapolation of $\xi(q^2)$.

VII. $|V_{us}|$ AND CKM UNITARITY

By combining with an estimate of $|V_{us}f_+(0)| = 0.2173(8)$ based on the recent experimental determination of Γ [3], we obtain

$$|V_{us}| = 0.2245(26)(8), \tag{45}$$

where the first and second errors come from the uncertainty in $f_+(0)$ and $|V_{us}f_+(0)|$, respectively. This leads to

$$|V_{ud}|^2 + |V_{us}|^2 + |V_{ub}|^2 = 1 - \delta, \qquad \delta = 0.0013(16), \tag{46}$$

which is completely consistent with CKM unitarity.

VIII. CONCLUSION

In this paper, we have calculated $f_+(0)$ from numerical simulations of two-flavor dynamical QCD using the domain-wall quark action. We obtained

$$f_+(0) = 0.968(9)(6), \qquad |V_{us}| = 0.2245(26)(8), \tag{47}$$

which supports CKM unitarity. While we have not estimated systematic uncertainties due to the use of the finite lattice spacing and the quenched approximation for strange quarks, these are expected to be small from the nice consistency with other lattice estimates.

Our result for $f_+(0)$ is consistent with the phenomenological estimate, which has been used in previous determinations of $|V_{us}|$, and hence has not changed $|V_{us}|$ significantly. The main significance of this study is that now $f_+(0)$ has been calculated nonperturbatively from two-flavor QCD and its uncertainties can be systematically reduced in future lattice calculations. Systematic errors which all the present lattice calculations share are those connected with the interpolation in momenta and extrapolation in mass. In both these cases it was necessary to use an ansatz. Since the interpolation in the momentum transfer was over a very small range, and the extrapolation in mass systematically took into account the calculated behavior up to NLO in ChPT, relying on the ansatz only for higher orders, both these effects are expected to be small.

However, it should be noted that the sea quark masses used in this calculation are relatively heavy, and to be confident that ChPT is a good description of the data it would be advisable to move to smaller masses. In turn this will make the momentum interpolation more difficult as $q^2_{\max}$ deviates further from 0. Another important step in the future is clearly an extension to dynamical three-flavor QCD. The RBC and UKQCD Collaborations' study of three-flavor QCD is well underway [48,49], and a more reliable estimate of systematic uncertainties in $f_+(0)$ will come in the near future.

ACKNOWLEDGMENTS

The authors would like to thank members of our RBC Collaboration and especially Norman Christ for many discussions and support. We also thank RIKEN, Brookhaven National Laboratory (BNL) and the U.S. Department of Energy for providing the facilities essential for this work. The work of T. K. is supported in part by the Grant-in-Aid of the Japanese Ministry of Education (No. 17740171). The work of A. S. was supported in part by US DOE Contract No. DE-AC02-98CH10886. T. K. is grateful to the Theory Group in BNL for their kind hospitality during his stay when this work was initiated.

[1] N. Cabibbo, Phys. Rev. Lett. **10**, 531 (1963); M. Kobayashi and T. Maskawa, Prog. Theor. Phys. **49**, 652 (1973).
[2] A. Czarnecki, W. J. Marciano, and A. Sirlin, Phys. Rev. D **70**, 093006 (2004).
[3] E. Blucher *et al.*, hep-ph/0512039.
[4] S. Eidelman *et al.*, Phys. Lett. B **592**, 1 (2004).
[5] L. Wolfenstein, Phys. Rev. Lett. **51**, 1945 (1983).
[6] N. Cabibbo, E. C. Swallow, and R. Winston, Annu. Rev. Nucl. Part. Sci. **53**, 39 (2003); D. Guadagnoli *et al.*, hep-ph/0606181.
[7] W. J. Marciano, Phys. Rev. Lett. **93**, 231803 (2004).
[8] E. Gámiz *et al.*, Phys. Rev. Lett. **94**, 011803 (2005).
[9] A. Sher *et al.*, Phys. Rev. Lett. **91**, 261802 (2003).
[10] T. Alexopoulos *et al.* (KTeV Collaboration), Phys. Rev. Lett. **93**, 181802 (2004); Phys. Rev. D **70**, 092006 (2004).
[11] A. Lai *et al.* (NA48 Collaboration), Phys. Lett. B **602**, 41 (2004).
[12] F. Ambrosino *et al.* (KLOE Collaboration), Phys. Lett. B **632**, 43 (2006).
[13] F. Ambrosino *et al.* (KLOE Collaboration), Phys. Lett. B **626**, 15 (2005).
[14] R. E. Behrends and A. Sirlin, Phys. Rev. Lett. **4**, 186 (1960); M. Ademollo and R. Gatto, Phys. Rev. Lett. **13**, 264 (1964).
[15] H. Leutwyler and M. Roos, Z. Phys. C **25**, 91 (1984).
[16] T. Takaishi, Phys. Rev. D **54**, 1050 (1996); Ph. de Forcrand *et al.* (QCD-TARO Collaboration), Nucl. Phys. **B577**, 263 (2000).
[17] D. B. Kaplan, Phys. Lett. B **288**, 342 (1992); R. Narayanan and H. Neuberger, Phys. Lett. B **302**, 62 (1993); Y. Shamir, Nucl. Phys. **B406**, 90 (1993); V. Furman and Y. Shamir, Nucl. Phys. **B439**, 54 (1995).
[18] T. Blum and A. Soni, Phys. Rev. Lett. **79**, 3595 (1997); Phys. Rev. D **56**, 174 (1997).
[19] S. Hashimoto *et al.*, Phys. Rev. D **61**, 014502 (1999).

[20] C. Dawson, T. Izubuchi, T. Kaneko, S. Sasaki, and A. Soni, PoS, LAT2005 (2006) 337.
[21] T. Alexopoulos *et al.* (KTeV Collaboration), Phys. Rev. D **70**, 092007 (2004).
[22] A. Lai *et al.* (NA48 Collaboration), Phys. Lett. B **604**, 1 (2004).
[23] O. P. Yushchenko *et al.*, Phys. Lett. B **589**, 111 (2004).
[24] A. Sirlin, Nucl. Phys. **B196**, 83 (1982).
[25] V. Cirigliano *et al.*, Eur. Phys. J. C **23**, 121 (2002); V. Cirigliano, H. Neufeld, and H. Pichl, *ibid.* **35**, 53 (2004).
[26] V. Bytev *et al.*, Eur. Phys. J. C **27**, 57 (2003); T. C. Andre, hep-ph/0406006.
[27] J. Gasser and H. Leutwyler, Nucl. Phys. **B250**, 517 (1985).
[28] J. Bijnens, G. Colangelo, and G. Ecker, Phys. Lett. B **441**, 437 (1998).
[29] P. Post and K. Schilcher, Eur. Phys. J. C **25**, 427 (2002).
[30] J. Bijnens and P. Talavera, Nucl. Phys. **B669**, 341 (2003).
[31] M. Jamin, J. A. Oller, and A. Pich, J. High Energy Phys. 02 (2004) 047.
[32] V. Cirigliano *et al.*, J. High Energy Phys. 04 (2005) 006.
[33] D. Bećirević *et al.*, Nucl. Phys. **B705**, 339 (2005); Eur. Phys. J. A **24S1**, 69 (2005).
[34] N. Tsutsui *et al.* (JLQCD Collaboration), PoS, LAT2005 (2005) 357.
[35] M. Okamoto (Fermilab, MILC and HPQCD Collaborations), hep-lat/0412044.
[36] P. F. Bedaque, Phys. Lett. B **593**, 82 (2004).
[37] D. Guadagnoli, F. Mescia, and S. Simula, Phys. Rev. D **73**, 114504 (2006).
[38] S. R. Sharpe and R. L. Singleton, Phys. Rev. D **58**, 074501 (1998); G. Rupak and N. Shoresh, Phys. Rev. D **66**, 054503 (2002); S. Aoki, Phys. Rev. D **68**, 054508 (2003).
[39] C. Aubin and C. Bernard, Phys. Rev. D **68**, 034014 (2003); **68**, 074011 (2003).
[40] T. Blum *et al.*, Phys. Rev. D **66**, 014504 (2002); **68**, 114506 (2003).
[41] R. Sommer *et al.* (ALPHA, CP-PACS and JLQCD Collaborations), Nucl. Phys. B, Proc. Suppl. **129**, 405 (2004); M. Della Morte, R. Hoffmann, F. Knechtli, and U. Wolf (ALPHA Collaboration), Comput. Phys. Commun. **165**, 49 (2005).
[42] A. Ali Khan *et al.* (CP-PACS Collaboration), Phys. Rev. D **64**, 114506 (2001).
[43] Y. Aoki *et al.*, Phys. Rev. D **73**, 094507 (2006).
[44] Y. Aoki *et al.*, Phys. Rev. D **69**, 074504 (2004).
[45] Y. Aoki *et al.*, Phys. Rev. D **72**, 114505 (2005).
[46] G. W. Kilcup *et al.*, Phys. Lett. B **164**, 347 (1985); C. Bernard *et al.*, in *Lattice Gauge Theory: A Challenge in Large-Scale Computing*, edited by B. Bunk *et al.* (Plenum, New York, 1986).
[47] D. Bećirević, G. Martinelli, and G. Villadoro, Phys. Lett. B **633**, 84 (2006).
[48] D. J. Antonio *et al.* (RBC and UKQCD Collaborations), PoS, LAT2005 (2005) 080.
[49] C. Dawson *et al.* (RBC and UKQCD Collaborations), Proc. Sci. LAT2006 (**2006**) 095; D. J. Antonio *et al.* (RBC and UKQCD Collaborations), Proc. Sci. LAT2006 (**2006**) 101.